Available online at www.sciencedirect.com

ScienceDirect

Ceramics International 40 (2014) 2153–2160

CERAMICS INTERNATIONAL

www.elsevier.com/locate/ceramint

Characterization of lead glazed potteries from Smyrna (İzmir/Turkey) using multiple analytical techniques; Part II: Body

M. Özçatal[a], M. Yaygıngöl[c], A. İssi[b,*], A. Kara[c], S. Turan[c], F. Okyar[c], Ş. Pfeiffer Taş[c], I. Nastova[d], O. Grupče[d], B. Minčeva-Šukarova[d]

[a]Afyon Kocatepe University, Faculty of Technology, Department of Metallurgical and Materials Engineering, Afyonkarahisar, Turkey
[b]Dumlupınar University, Department of Materials Science and Engineering, Kütahya, Turkey
[c]Anadolu University, Department of Materials Science and Engineering, Eskişehir, Turkey
[d]Ss. Cyril and Methodius University, Institute of Chemistry, Faculty of Natural Sciences and Mathematics, POB 162, 1001 Skopje, Republic of Macedonia

Received 14 June 2013; received in revised form 23 July 2013; accepted 27 July 2013
Available online 11 August 2013

Abstract

Lead glazed pottery was one of the most important ceramic ware groups for the Late Hellenistic, Roman, Byzantine and Ottoman cultures in Anatolia. They were produced in different places in Anatolia such as Tarsus, İznik, Smyrna, Clazomenae, Ephesus and Perge. This study represents the detailed study of 18 lead glazed potteries sherds excavated in Ayasuluk region (Smyrna) regarding the production technology. Different characterization techniques were applied: wavelength dispersive X-ray fluorescence (WDXRF) was performed for determination of the chemical content of the bodies, X-ray diffraction (XRD) and micro-Raman techniques were performed for mineralogical characterization of the sherds body, whereas scanning electron microscopy (SEM) with the combination of energy dispersive X-ray spectrometer (EDX) was performed for microstructural and microchemical characteristics of pottery sherds. Principle component analysis of the obtained WDXRF results of the potsherds bodies show that most of the sherds (except two) belong to the same group of potteries. XRD results showed that calcium-poor clays were used for the production of the bodies with firing temperature in a range from 600 to 1000 °C. Raman spectra provided information on the presence of minerals in bodies: carbon, graphite, albite, anatase, rutile, apatite, magnetite and several origin markers such as spessartine, phlogopite, hornblende, olivine and sphalerite.

Keywords: Archaeometrical characterization; Lead glazed pottery; Raman spectra of minerals; İzmir

1. Introduction

Archaeometrical studies for ceramics focus on some topics such as (i) dating (when was the artifact produced?), (ii) provenance (where was the artifact produced?) and (iii) technology (how was the artifact produced?). The results of systematic researches in archaeometry may contribute to the archaeological documentation. This seems to be an important piece of information about the development of ceramics manufacturing throughout history. Lead glazed pottery was one of the most important ceramic ware groups for the Late Hellenistic, Roman, Byzantine and Ottoman cultures in Anatolia [1,2]. The ease of production of these wares at relatively lower temperatures with the desired transparency and bright colored bodies were the main reasons for their preference [3]. There were many production centers for these wares in Anatolia such as Tarsus, İznik, Smyrna, Clazomenae, Ephesus and Perge [1,2,4,5]. Archeological excavations have brought to light some lead glazed pottery sherds at Ayasuluk region dated to XV–XVII centuries occupied by Byzantine and Ottoman cultures. This study was focused on production technology of pottery bodies, raw materials used in manufacturing, conditions and firing temperatures.

2. Materials and methods

Representative optical images and macro descriptions of lead glazed potsherds were already given in the first part of the study.

*Corresponding author. Tel.: +90 274 265 2031x4309; fax: +90 274 265 2066.
E-mail address: aliissi@hotmail.com (A. İssi).

0272-8842/$ - see front matter © 2013 Elsevier Ltd and Techna Group S.r.l. All rights reserved.
http://dx.doi.org/10.1016/j.ceramint.2013.07.132

Table 1
The chemical analysis results of bodies of the investigated samples (wt%).

Oxide/sample code	SiO_2	Al_2O_3	Fe_2O_3	Na_2O	K_2O	CaO	MgO	TiO_2	P_2O_5	SO_3	MnO	PbO
G1	50.31	23.13	12.18	2.03	4.64	1.33	4.48	1.07	0.23	0.04	0.16	0.12
G2	50.47	23.54	12.14	1.68	4.72	1.55	3.97	1.10	0.27	0.02	0.21	0.06
G3	51.99	22.29	11.70	1.84	4.46	1.78	4.03	1.10	0.27	0.03	0.18	0.13
G4	49.48	23.56	12.88	1.87	4.73	1.28	3.98	1.09	0.31	0.03	0.18	0.08
G5	52.74	22.34	11.25	2.05	4.68	1.15	3.82	1.02	0.24	0.04	0.15	0.28
G6	50.96	23.39	12.04	1.76	4.77	1.28	3.87	1.05	0.24	0.04	0.18	0.14
G7	50.53	22.70	11.93	1.76	4.75	1.39	3.63	0.95	0.26	0.05	0.16	1.64
G8	49.19	23.35	12.61	1.87	4.65	1.91	3.98	1.05	0.65	0.12	0.19	0.18
G9	49.60	22.08	11.89	2.06	4.56	2.62	4.24	1.04	1.30	0.09	0.13	0.13
G10	50.90	22.63	11.59	1.89	4.77	1.69	3.96	1.28	0.32	0.04	0.16	0.22
G12	50.00	23.30	12.62	1.78	4.60	1.29	4.14	1.06	0.26	0.02	0.18	0.52
K1	50.64	23.25	12.27	1.79	4.95	1.36	3.87	1.09	0.26	0.03	0.16	0.08
K2	50.46	23.19	12.46	1.96	4.64	1.31	4.05	1.00	0.27	0.02	0.15	0.29
K3	49.73	22.96	12.29	1.87	4.71	1.31	4.03	1.10	0.26	0.01	0.15	1.36
K4	54.29	18.96	8.84	2.05	4.20	5.18	4.44	0.10	0.21	0.05	0.13	0.45
K5	60.41	16.29	8.27	0.09	2.69	6.19	3.68	0.93	0.18	0.07	0.15	0.05
K6	50.28	23.28	12.23	1.76	4.65	1.37	4.51	1.07	0.26	0.04	0.17	0.06

2.1. Chemical and phase analysis

A Rigaku ZSX Primus Wavelength Dispersive X-ray Fluorescence instrument (WDXRF) was used for chemical analysis of major and minor elements present in the bodies. Glass tablets were prepared by fluxing for the measurement with a ratio of 1:10 powder: $Li_2B_4O_7$ in weight. Calculation of the quantity of elements and converting these to oxide contents in semi-quantitative scale was conducted with ZSX software.

A powder diffractometer (Rigaku Rint 2200) with Cu Kα radiation (λ=1.5418 Å) and a secondary graphite monochromator were used for the mineralogical analysis. XRD spectra were obtained by scanning from 5 ° to 70 ° angles (2θ), with a goniometer speed of 2 °/min, 40 kV acceleration voltage and 30 mA current. Sampling width was 0.02 °. The interpretation of phase content of the data was conducted with Jade 7 software by searching and matching with JCPDS files.

2.2. Microstructural and microchemical characterization

Potsherds were cut to obtain body-glaze cross-sectional samples. These samples were mounted with the vacuum impregnation method and were polished to have flat surfaces prior to SEM investigation. Samples were examined uncoated in a variable pressure field emission gun SEM (Zeiss Supra 50VP) attached with an energy dispersive X-ray (EDX-Oxford Instruments) spectrometer under 20 kV with 8 mm working distance (WD).

2.3. Micro-Raman spectroscopy

Micro-Raman multichannel spectrometer, (LabRam 300 Horiba Jobin-Yvon) equipped with frequency-doubled Nd: YAG laser operating at 532 nm and with an excitation power of around 5 mW at the sample was used for recording Raman spectra in 100 to 2000 cm^{-1} region. An Olympus MPlaN microscope, with magnification of 50 × and 50 × LWD was used to focus the laser onto the sample. The backscattered light was dispersed using 1800 lines/mm grating. The spectral resolution was around 3 cm^{-1}. Acquisition times were between 5 and 10 s, with 10–20 scans. The laser diameter on the samples was 2 μm. The LABSPEC package [6] was used for spectra acquisition and GRAMS 32 for spectra manipulation [7]. All spectra were baseline corrected and filtered if needed with LABSPEC software to remove the background fluorescence and excessive noise.

Point-to-point micro-Raman spectroscopy with XY motorized mapping stage was applied in assessment of the mineralogical composition of the ceramic body. Pellets prepared from approximately 200 mg of powdered body were placed under the microscope (50 ×) on a mapping stage covering an area of 0.04 × 0.04 mm^2 up to 0.07 × 0.07 mm^2. Each spectrum was recorded in 6–8 μm steps yielding around 100 Raman spectra from each selected spot. The Raman spectra were then analyzed using different databases of minerals [8].

3. Results and discussion

3.1. Chemical and phase characterization

The chemical analysis results of 18 samples were given in Table 1. As it has been already determined, Symrna lead-glazed potteries dated to first century BC and first century AD periods were made from non-calcareous clays [2]. According to the results, the potsherds have an iron-rich composition with Fe_2O_3 quantities changing from 8.27 to 12.88 wt%. Quantities of Na_2O and K_2O were in a moderate range from 0.09 to 2.06 wt% and 2.69 to 4.95 wt%, respectively. Quantities of CaO and MgO were between 1.15 and 6.19 wt% and 3.63 and 4.51 wt%, respectively. These contents could be determined by the conditions of formation of clays in the geological environment. Clay deposits may contain natural ingredients

such as quartz, feldspars, iron minerals, calcium-rich materials and organic residues [9]. Na_2O and K_2O quantities should be provided by clay minerals such as illite/muscovite and the other components in clay, especially feldspars. The change in the quantity of CaO is more pronounced than in MgO. It may suggest that the source of CaO is not only from dolomitic materials but from the calcareous materials as well. Trace elements below 0.1% in weight are not given in Table 1 since they are below the reliable detection limits of the instrument. The quantities of trace elements change between 0.01 and 0.09 wt% for SO_3, 0.04 and 0.08 wt% for Cr_2O_3, 0.02 and 0.05 wt% for NiO, 0.02 and 0.05 wt% for CuO, 0.02 and 0.03 wt% for ZnO, 0.04 and 0.07 wt% for Rb_2O, 0.02 and 0.04 wt% for SrO, 0.03 and 0.04 wt% for ZrO_2. Quantities of SiO_2 versus Fe_2O_3, Na_2O, K_2O, CaO and MgO were plotted in Fig. 1. The correlation between these oxides concludes a cluster of potteries except two samples. The chemical compositions of K4 and K5 showed different quantities than the others in plots. It may be suggested that possible raw material source is different for K4 and K5 than the others.

XRD results of the potsherds are given in Table 2. Quartz (SiO_2), plagioclase (albite/anorthite) [$(Na_{1.0-0.9}Ca_{0.0-0.1}Al_{1.0-1.1}Si_{3.0-2.9}O_8)/(Na_{0.1-0.0}Ca_{0.9-1.0}Al_{1.9-2.0}Si_{2.1-2.0}O_8)$], alkali feldspar (microcline) ($KAlSi_3O_8$), illite/muscovite [$(K,H_3O)Al_2Si_3AlO_{10}(OH)_2$]/[$(K,Na)(Al,Mg,Fe)_2(Si_{3.1}Al_{0.9})O_{10}(OH)_2$], mica (phlogopite) ($KMg_3(Si_3Al)O_{10}(F,OH)_2$), dolomite $CaMg(CO_3)_2$, calcite ($CaCO_3$), melilite (akermanite) ($Ca_2MgSi_2O_7$), iron minerals (hematite/maghemite) [$(\alpha\text{-}Fe_2O_3)/(\gamma\text{-}Fe_2O_3)$] and spinels [$(FeAl_2O_4)$, $(Mg)(Al,Fe)_2O_4/MgAl_2O_4$] were identified in the samples.

Phase contents of the samples enable to estimate firing temperatures [10–13]. For example, illite/muscovite or mica structure breaks down in the range of 900–1000 °C [14–17].

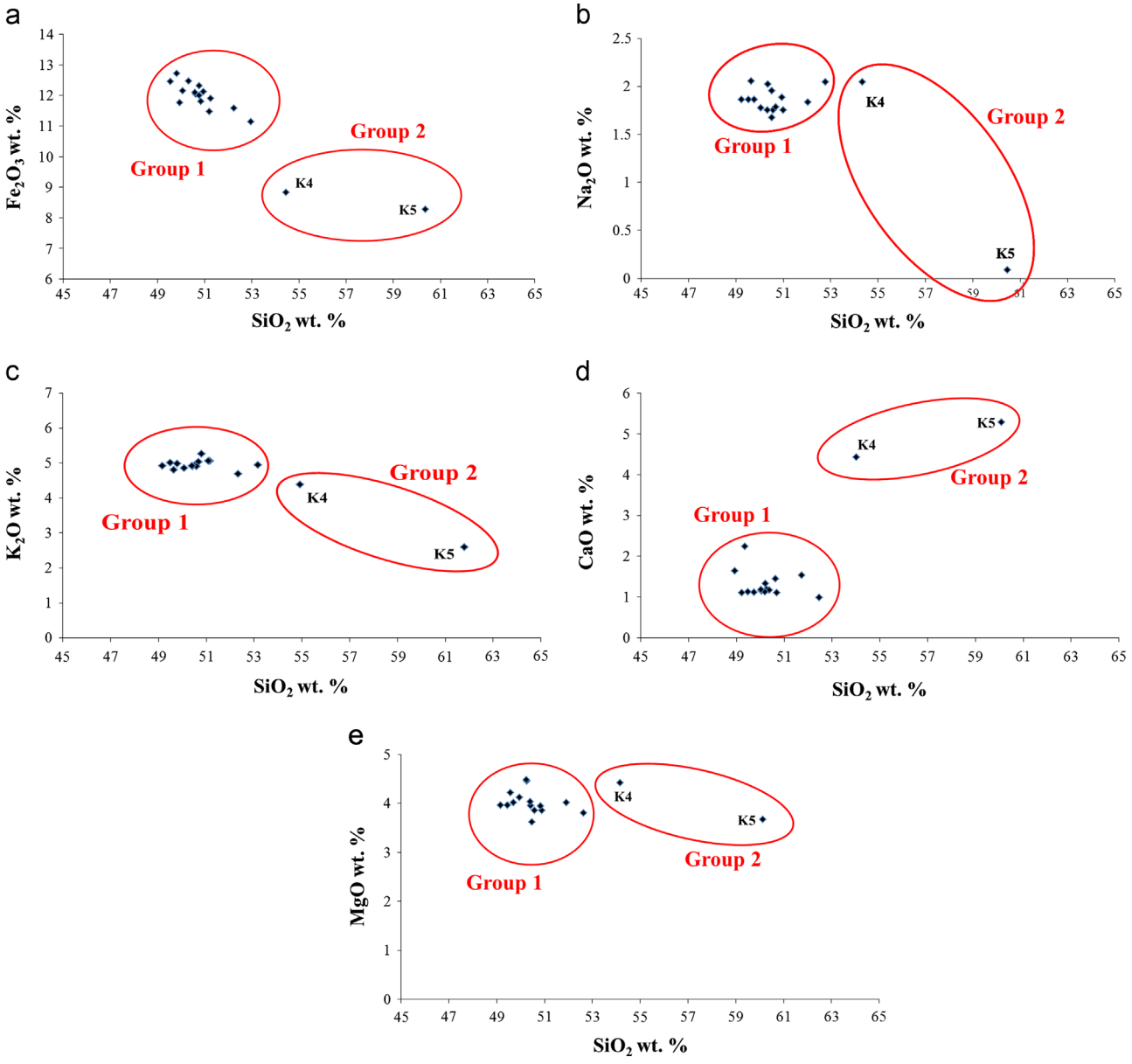

Fig. 1. Principle component analysis of SiO_2 versus (a) Fe_2O_3, (b) Na_2O, (c) K_2O, (d) CaO and (e) MgO.

Table 2
XRD results and estimated firing temperatures of the potsherds.

Sample code	Mineralogical/phase content	Estimated firing temperature (°C)
G1	Quartz, plagioclase (albite/anorthite), K-feldspar (microcline), Clay minerals (illite/muscovite), İron minerals (hematite, maghemite)	600–700
G2	Quartz, plagioclase (albite/anorthite), K-feldspar (microcline), Clay minerals (illite/muscovite), İron minerals (hematite, maghemite), Spinels [($FeAl_2O_4$), $(Mg)(Al,Fe)_2O_4$/$MgAl_2O_4$]	900–950
G3	Quartz, plagioclase (albite/anorthite), K-feldspar (microcline), melilite (akermanite), iron minerals (hematite, maghemite), Spinels [$(Mg)(Al,Fe)_2O_4/MgAl_2O_4$]	900–950
G4	Quartz, plagioclase (albite/anorthite), K-feldspar (microcline), Clay minerals (illite/muscovite), Carbonated minerals (dolomite), İron minerals (hematite, maghemite), Spinels [$(Mg)(Al,Fe)_2O_4/MgAl_2O_4$]	900–950
G5	Quartz, plagioclase (albite/anorthite), K-feldspar (microcline), Clay minerals (illite/muscovite), İron minerals (hematite, maghemite)	600–700
G6	Quartz, plagioclase (albite/anorthite), K-feldspar (microcline), Clay minerals (illite/muscovite), İron minerals (hematite, maghemite)	600–700
G7	Quartz, plagioclase (albite/anorthite), K-feldspar (microcline), Clay minerals (illite/muscovite), İron minerals (hematite, maghemite)	600–700
G8	Quartz, plagioclase (albite/anorthite), K-feldspar (microcline), Clay minerals (illite/muscovite), Melilite (gehlenite), Iron minerals (hematite, maghemite), Spinels [$(Mg)(Al,Fe)_2O_4/MgAl_2O_4$]	900–950
G9	Quartz, plagioclase (albite/anorthite), K-feldspar (microcline), Clay minerals (illite/muscovite), İron minerals (hematite, maghemite)	600–700
G10	Quartz, plagioclase (albite/anorthite), K-feldspar (microcline), Clay minerals (illite/muscovite), Melilite (akermanite), İron minerals (hematite, maghemite)	900–950
G11	Quartz, plagioclase (albite/anorthite), K-feldspar (microcline), Clay minerals (illite/muscovite), İron minerals (hematite, maghemite), Melilite (akermanite), hercynite ($FeO.Al_2O_3$), Spinels [$(Mg)(Al,Fe)_2O_4/MgAl_2O_4$]	950–1000
G12	Quartz, plagioclase (albite/anorthite), K-feldspar (microcline), Clay minerals (illite/muscovite), İron minerals (hematite, maghemite), Spinel ($FeAl_2O_4$)	900–950
K1	Quartz, plagioclase (albite/anorthite), K-feldspar (microcline), Clay minerals (illite/muscovite), mica, Melilite (akermanite), İron minerals (hematite, maghemite), Spinel ($FeAl_2O_4$)	900–950
K2	Quartz, plagioclase (albite/anorthite), K-feldspar (microcline), Clay minerals (illite/muscovite), Carbonated minerals (dolomite), Melilite (akermanite), İron minerals (hematite, maghemite),	800–850
K3	Quartz, plagioclase (albite/anorthite), K-feldspar (microcline), Clay minerals (illite/muscovite), Melilite (akermanite), İron minerals (hematite, maghemite), Spinel ($FeAl_2O_4$)	900–950
K4	Quartz, plagioclase (albite/anorthite), K-feldspar (microcline), Clay minerals (illite/muscovite), Carbonated mineral (dolomite), İron minerals (hematite, maghemite)	600–700
K5	Quartz, plagioclase (albite/anorthite), K-feldspar (microcline), Clay minerals (illite/muscovite), İron minerals (hematite, maghemite)	800–850
K6	Quartz, plagioclase (albite/anorthite), K-feldspar (microcline), Clay minerals (illite/muscovite), Melilite (akermanite), İron minerals (hematite, maghemite)	600–700

If the firing temperature does not exceed this range, these minerals still continue to exist as the components of the potsherds. With ascending of the firing temperature the illite is disintegrated but an intermediate phase between spinel ($MgO \cdot Al_2O_3$) and hercynite ($FeO \cdot Al_2O_3$) is formed [18]. The formation of spinel phases is affected by the presence or absence of interlayer cations, substitutional impurities and accessory minerals in clays [19]. Calcite decomposition into CaO and CO_2 begins around 650 °C and it is completed up to 900 °C. Trindade et al. concluded that the decarbonation of calcite may extend to 1100 °C for calcite rich systems [20]. On the other hand, secondary calcite may occur in ceramics as a result of post-burial deposition processes due to recarbonation of lime [21]. Dolomite decomposes in two stages beginning at around 650 °C. After the decomposition of dolomite into calcite and magnesite, decarbonation of dolomite is completed up to 750–800 °C [14,16,22]. On the other hand, identification

of calcite as a transient phase at this stage is difficult by conventional diffraction methods [23]. Quartz and feldspars can persist up to 1000 °C [9]. Pyroxenes like diopside and augite may be generated from dolomite and silica reactions at 800–900 °C. Gehlenite may be formed at 850 °C with the reaction of CaO and illite structure [24]. Iron minerals found in the samples may help in assessing the firing atmosphere [25,26]. All the samples contain hematite. It may suggest that firing cycle ended in oxidative condition. However, presence of maghemite is identified in several sherds which may suggest reducing atmosphere. The possibility, both oxidative and reducing atmosphere during firing of these potsherds should not be excluded. Although the presence of maghemite in the raw materials cannot be excluded either, since its existence in the natural raw materials is scanty, it was most probably obtained during firing [27]. Occurrence of maghemite may have been also caused due to the difference in temperature reached in the pottery depending on the thickness of the body even in cases when the ware was placed in a uniform flame of firing [28]. However, the presence of low temperature minerals and high temperature phases such as dolomite and spinels together should be the indication of different firing temperatures during firing either in single or double steps. Furthermore, it is difficult to conclude if glaze was applied after bisque firing of ceramics.

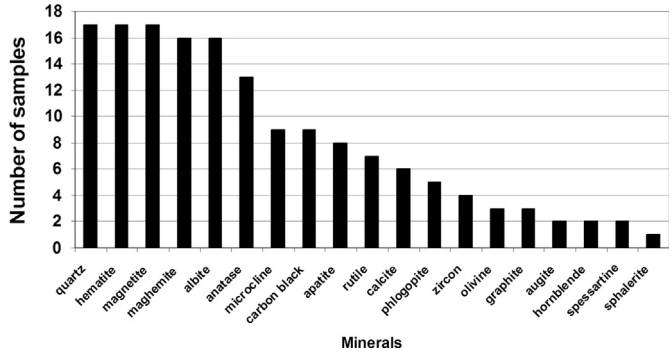

Fig. 2. Cumulative graph of identified minerals as well as frequency of their occurrence in the analyzed samples.

3.2. Micro-Raman spectroscopy

Micro-Raman spectroscopy provides complementary information on the mineralogical composition of the ceramic sherds [29]. While the results from the XRD spectra provided detailed information on the clay and other relevant crystalline minerals, Raman spectra provided additional information on the amorphous minerals and minerals present in amounts less than 2 wt%. Since the Raman spectra were recorded from a pellet of powdered ceramic body, about hundred spectra from each selected area on the pellet surface were recorded and analyzed. Pure minerals or mixture of minerals were identified. The cumulative graph of all the identified minerals as well as frequency of their occurrence is given in Fig. 2 while representative Raman spectra of the selected minerals are shown in Fig. 3.

When Raman spectra of the ceramic bodies are compared with the results obtained from the XRD analysis, it is obvious that the most abundant minerals identified in all the samples, both by XRD and Raman spectra, are quartz, feldspars and iron oxides. Quartz was readily identified by its prominent Raman peak at 461 cm^{-1} and a medium intensity peaks at 200 and 124 cm^{-1}, while hematite (α-Fe_2O_3), was characterized by Raman bands at 220, 285, 401 and 1308 cm^{-1}. It is worth mentioning that in some of the samples, the change of the wave numbers, as well as the change of the shape and/or broadening of the hematite Raman bands was observed. This could be due to variation in crystallinity, the grain size or to the partial Fe/M substitution [30]. Besides, hematite, maghemite (γ-Fe_2O_3) and magnetite (Fe_3O_4) were often identified. The presence of maghemite (346, 503, 715 cm^{-1}) and magnetite (665 cm^{-1}), together with the identified carbon could suggest reduction firing atmosphere at some point

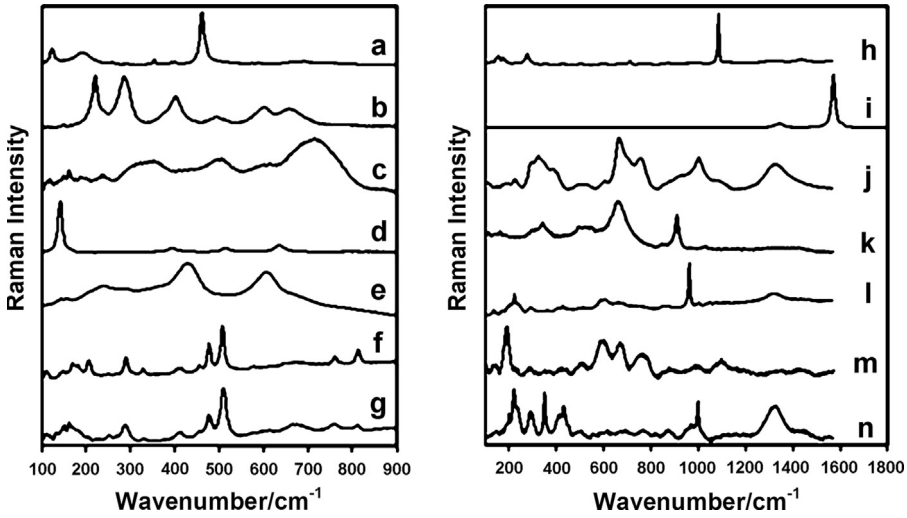

Fig. 3. Raman spectra of selected minerals, identified in the ceramic bodies: (a) quartz (SiO_2); (b) hematite (α-Fe_2O_3) and magnetite ($Fe^{2+}Fe_2^{3+}O_4$); (c) maghemite (γ-Fe_2O_3); (d) anatase (TiO_2); (e) rutile (TiO_2); (f) Albite ($Na_{1.0-0.9}Ca_{0.0-0.1}Al_{1.0-1.1}Si_{3.0-2.9}O_8$); (g) Microcline ($KAlSi_3O_8$); (h) calcite ($CaCO_3$); (i) graphite (C); (j) augite ($(Ca,Na)(Mg,Fe,Al,Ti)(Si,Al)_2O_6$); (k) spessartine ($Mn_3^{2+}Al_2(SiO_4)_3$); (l) apatite; (m) phlogopite ($KMg_3Si_3AlO_{10}(FOH)_2$) and (n) sphalerite ((Zn, Fe)S).

of the firing. Since the analyzed samples are red ware, it could also suggest double firing – one for the biscuit (higher and possibly reductive) and second for the glaze, being oxidizing.

Characteristic Raman signals also provide means for feldspars identification: plagioclase feldspars have characteristic vibrational modes between 500 and 510 cm^{-1} while in alkali feldspars most intensive band appears in the spectrum around 514 cm^{-1} [31]. The most common type of feldspar, albite, was identified in most of the samples, but in several samples microcline was also detected. Although both minerals were found, the Raman spectra suggested that albite is more abundant mineral than microcline in the analyzed samples.

In majority of samples, the presence of carbon black (amorphous carbon, characterized by two broad peaks around 1340 and 1600 cm^{-1}) was identified. It may originate from the added wood or bone ash to the sand and clay as a fluxing agent during the preparation of the paste [1–4]. However, latter burning of the ceramics, which will also lead to amorphous carbon deposition, could not be excluded. In addition to carbon black, graphite (sharp band at 1572 cm^{-1} accompanied with wide, small band at 1343 cm^{-1}) was identified in several samples as well. Its presence could be related to the thermal transformation of the existing non-crystalline carbon in the ceramic body, at least partly, into crystalline graphite. The presence of graphite could be a confirmation of higher firing temperature of these samples, which corresponds with the proposed high firing temperature (900–950 °C) of the samples G10 and G12 where graphite was identified. The presence of both allotropes of carbon could be indication of reducing firing atmosphere as well [32].

In approximately half of the samples, apatite was identified, by the characteristic peak of phosphate group (962 cm^{-1}). The presence of apatite could be related to the charred bones used in the preparation of clay, as already discussed regarding to the presence of carbon. However, latter contamination, either by the food that was prepared and/or kept in the vessels or by organic contamination during the period the sherds were buried in the ground cannot be excluded.

It is known that micro-Raman spectroscopy can provide information on the compounds present in small amount, and even in traces. Although XRF analysis of the bodies has shown that TiO_2 is maximum 1.28 wt% (Table 1), its presence can be easily identified by the Raman spectra due to the high Raman scattering [33]. One of the polymorphs of TiO_2, anatase, was identified in almost all the samples (except for the G12 sample) while rutile, the other TiO_2 polymorph, was found mainly in sherds fired at higher temperatures. Presence of rutile in G5 and G6, fired at lower temperatures, indicates that rutile probably was present in raw material as constituent and is probably not the transformation product from anatase during the firing of the pottery.

The presence of pyroxene group minerals, augite [$(Ca,Na)(Mg,Fe,Al,Ti)(Si,Al)_2O_6$] and zircon ($ZrSiO_4$) were also identified in some of the samples, as well as spessartine ($Mn_3^{2+}Al_2(SiO_4)_3$), phlogopite ($KMg_3Si_3AlO_{10}(F,OH)_2$), hornblende, olivine and sphalerite ((Zn, Fe)S). Some of these minerals are not commonly found in clays and could serve as discriminative, provenance related, minerals.

3.3. Microstructural and microchemical analysis

The BSE images of three representative samples; G7 (600–700 °C), G3 (900–950 °C) and G11 (950–1000 °C), which

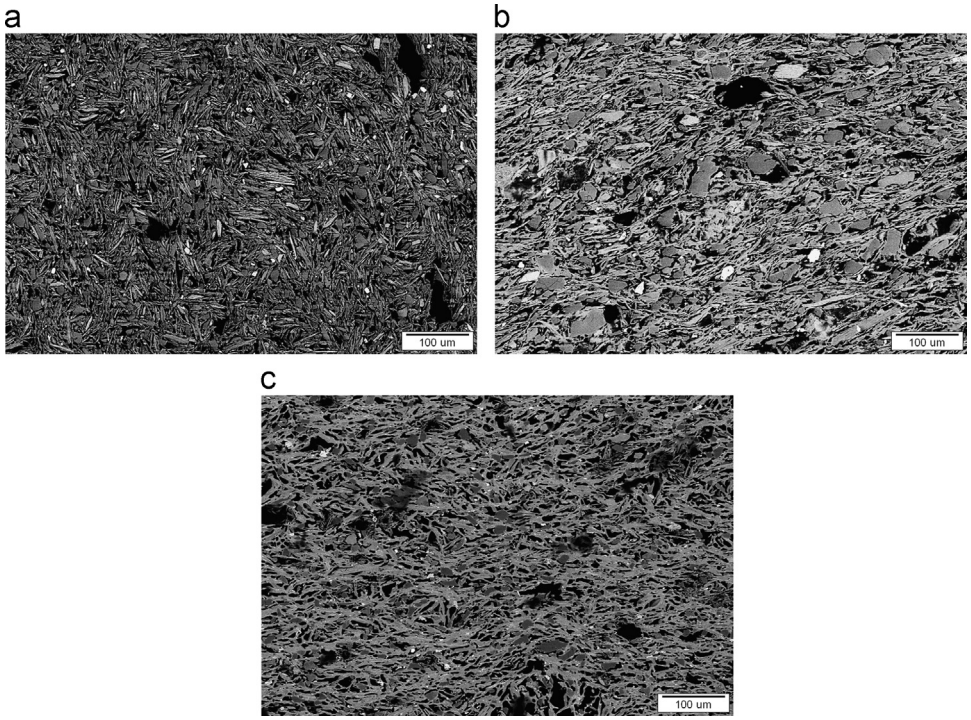

Fig. 4. (a) G7, (b) G3 and (c) G12 representative back scattered SEM images taken from polished surfaces of the samples.

were exposed to different firing temperatures determined from XRD and Raman spectra are given in Fig. 4.

The estimated firing temperatures of the bodies were confirmed from the BSE images. If the firing temperature increased, the grains started to fuse into each other, and sharp grains became smoother [34]. A homogenous grain size distribution can be seen in the microstructure of the G11 sample exposed the highest firing temperature in Fig. 4c. In addition, the absence of very coarse grains in the microstructure shows that the raw materials may originate from sedimentary rocks [35]. Some residual quartz grains were observed in the SEM images. They may be originated from raw materials. Quartz and feldspar grains may persist up to 1000 °C [36]. In general, melting behavior of any quartz grains was not observed in the microstructures. Therefore, it may be concluded that the firing temperature never exceeded 1000 °C.

4. Conclusions

Principle component analysis of major and minor oxides for the body of the potsherds showed a cluster of potteries except two samples. Iron-rich, non-calcareous illitic clays were used to produce potteries from Smyrna. It may be suggested that traditional approach for lead glazed ceramic body manufacturing around Symrna has similar characteristics with earlier ones dated to first century BC. Mineralogical and phase content of the potsherds suggested that firing temperatures varied between 600 and 1000 °C. The presence of low temperature minerals and high temperature phases such as dolomite and spinels together should be the indication of different firing temperatures during firing either in single or double steps. Since the analyzed samples are reddish in color, firing cycles should be performed in double firing: one for the biscuit (higher and possibly reductive) and second for the glaze (lower and possibly oxidizing). However, regular shape of quartz and feldspar grains in the samples suggested to conclude the firing temperature never exceeded 1000 °C.

Acknowledgments

Financial support by the Scientific and Technological Research Council of Turkey (TÜBİTAK) with the Project number of 108M386 and Ministry of Education and Science, Republic of Macedonia Macedonian–Turkish bilateral Project titled “Byzantine and Early Ottoman Artifacts in Republic of Macedonia and Turkey: Characterization and Comparisons” is acknowledged.

References

[1] A.P. Kazhdan, A.W. Epstein, Change in Byzantine Culture in the Eleventh and Twelfth Centuries, University of California Press, London 70–71.
[2] M.S. Walton, M.S. Tite, Production technology of Roman lead-glazed pottery and its continuance into late antiquity, Archaeometry 52 (2010) 733–759.
[3] M.S. Tite, I. Freestone, R. Mason, J. Molera, M. Vendrell-Saz, N. Wood, Lead glazes in antiquity-methods of production and reasons for use, Archaeometry 40 (1998) 241–260.
[4] K. Greene, Late hellenistic and early Roman invention and innovation: the case of lead-glazed pottery, American Journal of Archaeology 111 (2007) 653–671.
[5] G. Simsek, P. Colomban, V. Milande, Tentative differentiation between Iznik tiles and copies with Raman spectroscopy using both laboratory and portable instruments, Journal of Raman Spectroscopy 41 (2009) 529–536.
[6] LabSpec, LabSpec Version 5.25.15, 2007.
[7] Galactic Industries Corporation, GRAMS/32 Spectral Notebase Version 4.10, 1996.
[8] Thermo Galactic, Spectral ID (3.02), 2003.
[9] A. Iordanidis, J. Garcia-Guinea, G. Karamitrou-Mentessidi, Analytical study of ancient pottery from the archaeological site of Aiani, Northern Greece, Materials Characterization 60 (2009) 292–302.
[10] S. Wolf, Estimation of the Production Parameters of Very Large Medieval Bricks from St. Urban, Archaeometry, Switzerland37–65.
[11] G. Velraja, K. Janakia, A.M. Musthafaa, R. Palanivelb, Estimation of firing temperature of some archaeological pottery sherds excavated recently in Tamilnadu, India, Spectrochimica Acta A 72 (2009) 730–733.
[12] R. Palanivel, U.R. Kumar, The mineralogical and fabric analysis of ancient pottery artifacts, Cerâmica 57 (2011) 56–62.
[13] L. Damjanović, I. Holclajtner-Antunović, U.B. Mioč, V. Bikić, D. Milovanović, I.R. Evans, Archaeometric study of medieval pottery excavated at Stari (Old) Ras, Serbia, Journal of Archaeological Science 38 (2011) 818–828.
[14] C. Papachristodoulou, A. Oikonomou, K. Ioannides, K. Gravani, A study of ancient pottery by means of X-ray fluorescence spectroscopy, multivariate statistics and mineralogical analysis, Analytica Chimica Acta 573 (2006) 347–353.
[15] R.W. Grimshaw, Reactions at High Temperatures, The Chemistry and Physics of Clays, Techbooks, India 727.
[16] L. Maritan, C. Mazzoli, L. Nodari, U. Russo, Second iron age grey pottery from Este (northeastern Italy): study of provenance and technology, Applied Clay Science 29 (2005) 31–44.
[17] J.M. Bhatnagar, R.K. Goel, Thermal changes in clay products from alluvial deposits of the Indo-Gangetic plains, Construction and Building Materials 16 (2002) 113–122.
[18] M.M. Jordán, A. Boix, T. Sanfeliu, C. de la Fuente, Firing transformations of cretaceous clays used in the manufacturing of ceramic tiles, Applied Clay Science 14 (1999) 225–234.
[19] C.J. McConville, W.E. Lee, Microstructural development on firing illite and smectite clays compared with that in kaolinite, Journal of the American Ceramic Society 88 (2005) 2267–2276.
[20] M.J. Trindade, M.I. Dias, J. Coroado, F. Rocha, Mineralogical transformations of calcareous rich clays with firing: a comparative study between calcite and dolomite rich clays from Algarve, Portugal, Applied Clay Science 42 (2009) 345–355.
[21] J. Buxeda, I Garrigós, H. Mommsen, A. Tsolakidou, Alterations of Na, K and Rb concentrations in Mycenaean pottery and a proposed explanation using X-ray diffraction, Archaeometry 44 (2002) 187–198.
[22] S. Shoval, Using FT-IR spectroscopy for study of calcareous ancient ceramics, Optical Materials 24 (2003) 117–122.
[23] A.H. De Aza, X. Turrillas, J.L. Rodríguez, P. Pena, Estudio del proceso de sinterización reactiva en sistemas con dolomita mediante termodifractometría de neutrones, Boletin de la Sociedad Espanola de Ceramica 43 (2004) 12–15.
[24] G. Cultrone, C. Rodriguez-Navarro, E. Sebastian, O. Cazalla, M.J. De La Torre, Carbonate and silicate phase reactions during ceramic firing, European Journal of Mineralogy 13 (2001) 621–634.
[25] J. van der Weerd, G.D. Smith, S. Firth, R.J.H. Clark, Identification of black pigments on prehistoric Southwest American potsherds by infrared and Raman microscopy, Journal of Archaeological Science 31 (2004) 1429–1437.
[26] C.C. Tang, E.J. MacLean, M.A. Roberts, D.T. Clarke, E. Pantos, A.J. N. Prag, The study of Attic black gloss sherds using synchrotron x-ray diffraction, Journal of Archaeological Science 28 (2001) 1015–1024.

[27] P.R.S. Moorey, Ancient Mesopotamian Materials and Industries, The Archaeological Evidence, Oxford University Press, New York 152–156.
[28] M. Maggetti, Ch. Neururer, D. Ramseyer, Temperature evolution inside a pot during experimental surface (bonfire) firing, Applied Clay Science 53 (2011) 500–508.
[29] B. Minčeva-Šukarova, A. İssi, A. Raškovska, O. Grupče, V. Tanevska, M. Yaygıngöl, A. Kara, P. Colomban, Characterization of pottery from Republic of Macedonia III. a study of comparative mineralogical detection efficiency using micro-Raman mapping and X-ray diffraction, Journal of Raman Spectroscopy 43 (2012) 792–798.
[30] F. Froment, A. Tournié, P. Colomban, Raman identification of natural red to yellow pigments: ochre and iron-containing ores, Journal of Raman Spectroscopy 39 (2008) 560–568.
[31] T.P. Mernagh, Use of the laser Raman microprobe for discrimination amongst feldspar minerals, Journal of Raman Spectroscopy 22 (1991) 453–457.
[32] J.M. Pérez, R. Esteve-Tébar, Pigment identification in Greek pottery by Raman microspectroscopy, Archaeometry 46 (2004) 607–614.
[33] R.J.H. Clark, Q. Wang, A. Correia, Can the Raman spectrum of anatase in artwork and archaeology be used for dating purposes? Identification by Raman microscopy of anatase in decorative coatings on Neolithic (Yangshao) pottery from Henan, China, Journal of Archaeological Science 34 (2007) 1787–1793.
[34] R. Palanivel, S. Meyvel, Microstructural and microanalytical study - (SEM) of archaeological pottery artefacts, Romanian Journal of Physics 55 (2010) 333–341.
[35] A.K. Marghussian, H. Fazeli, Chemical-mineralogical analyses and microstructural studies of prehistoric pottery from Rahmatabad, south-west Iran, Archaeometry 51 (2009) 733–747.
[36] A. Issi, A. Kara, A.O. Alp, An investigation of Hellenistic period pottery production technology from Harabezikan/Turkey, Ceramics International 37 (2011) 2575–2582.